Inclusion of Rainwater Budget and Convective Downdrafts in the Arakawa–Schubert Cumulus Parameterization

MING-DEAN CHENG

Central Weather Bureau, Taipei, Taiwan, Republic of China

AKIO ARAKAWA

Department of Atmospheric Sciences, University of California, Los Angeles, Los Angeles, California

(Manuscript received 6 May 1996, in final form 17 September 1996)

ABSTRACT

A combined updraft–downdraft model that includes the mass, rainwater, and vertical momentum budget equations for both updrafts and downdrafts is incorporated into the Arakawa–Schubert (A–S) cumulus parameterization. The model assumes that the rainwater generated in an updraft falls partly inside and partly outside the updraft. Two types of stationary solutions are identified for the coupled rainwater budget and vertical momentum equations: solutions for small tilting angles and solutions for large tilting angles. The balance of terms in the rainwater budget equation is quite different between these solutions, and solutions for small tilting angles are unstable, while solutions for large tilting angles are stable. The cause of the instability is interpreted, considering the effect of rain drag on the vertical transport of rainwater. The motivation for an optimum choice of the tilting angle for use in the revised parameterization is discussed. The results of semiprognostic and single-column prognostic tests of the revised A–S parameterization using the GATE Phase III data show drastic improvement in predicting the humidity field through the inclusion of downdraft effects. An updraft model with a simplified rainwater budget equation, which is used in the authors' current GCM applications of the revised parameterization, is also presented.

1. Introduction

The Arakawa–Schubert cumulus parameterization [Arakawa and Schubert (1974), hereafter referred to as A–S; see also Arakawa and Cheng (1993)] combines a spectral cumulus ensemble model with a closure assumption on the quasi equilibrium of cloud work function (see also Lord and Arakawa 1980; Lord 1982; Lord et al. 1982). In its original form, the cumulus ensemble model does not include convective downdrafts, which are a significant component of virtually all convective systems. For a given updraft mass flux, convective downdrafts tend to decrease the cumulus heating and drying above cloud base through a reduction of the subsidence between clouds. The outflow from downdrafts below cloud base, on the other hand, tends to cool and dry the subcloud layer. Implementing these downdraft effects, therefore, is an important step to further improve the cumulus parameterization.

Among various types of convective downdrafts, those associated with precipitation seem to be the most important for the large-scale heat and moisture budgets (Knupp and Cotten 1985; Houze 1989). These downdrafts are initiated and maintained by the loading and cooling due to the evaporation of precipitation. For determining the properties of downdrafts, therefore, it is essential to formulate how precipitation detrains from updrafts.

Johnson (1976) made the first attempt to include the downdraft effects by incorporating inverted plumes into the cumulus ensemble model. As later pointed out by Payne (1981), at least six free parameters are required to fully determine the properties of a downdraft plume. They are the height of the (inverted) plume top, the mass flux at the plume top, the entrainment and detrainment rates of the plume, the properties of the entrained air, the relative humidity of the plume, and the height of the plume base. In applying the inverted-plume downdraft model to studies of cumulus convection, Johnson (1976, 1980), Fritsch and Chappel (1980), Payne (1981), Molinari and Corsetti (1985), Kao and Ogura (1987), Grell et al. (1991), Grell (1993), and Pan and Wu (1994) made their own selections of these parameters. To refine the formulation of entrainment, Frank and Cohen (1987) included the vertical momentum equation in their convective downdraft model, in which an empirical parameter is used to determine the partition

Corresponding author address: Dr. Akio Arakawa, Department of Atmospheric Sciences, University of California, Los Angeles, 405 Hilgard Avenue, Los Angeles, CA 90095.
E-mail: aar@atmos.ucla.edu

of the rainfall between convective downdraft and its environment. Emanuel (1991) calculated dynamical entrainment into the downdraft through applications of the vertical momentum and energy budget equations for the downdraft. The evaporation of rainwater within the downdraft was also included in his model. Sud and Walker (1993), on the other hand, developed a simpler downdraft model for use in their general circulation model. In all of these studies the intensity of downdrafts is determined without explicitly calculating the precipitation budget for the associated updrafts.

Srivastava (1985, 1987) showed that a one-dimensional downdraft model can simulate downdrafts with various intensities depending on the amount of raindrops and ice particles supplied through the downdraft top. Haman and Niewiadomski (1980), on the other hand, developed a one-dimensional updraft–downdraft cloud model. In their model, cloud water carried by updraft air is entrained into the downdraft according to a specified lateral entrainment rate that depends on the difference of the updraft and downdraft velocities. They found, however, that the effects of entrainment alone cannot maintain the downdraft, especially within the lower portion of the cloud layer. They thus concluded that a certain amount of additional precipitation supply, resulting from a slanted interface between the updraft and downdraft for example, is needed to simulate downdrafts with reasonable intensity. Little was known, however, about how the tilt of updrafts can be determined for a given environmental condition.

Using a time-dependent two-dimensional cloud model, Seitter and Kuo (1983) discussed a possible mechanism by which the drag of precipitation may affect the tilt of convective clouds. Using a linear analytical cloud model, Emanuel (1986) further demonstrated the crucial effect of precipitation loading in the cloud layer, as well as the evaporation of precipitation within the subcloud layer, on the instability of sloping moist convection. Consequently, he found that the instability depends on the tilt of the cloud. Without addressing the cause of cloud tilting, on the other hand, Ferrier and Houze (1989) constructed a one-dimensional time-dependent cloud model that includes a parameter representing the tilt of the cloud. They demonstrated with their model that the tilt allows the updraft to develop more deeply and generate stronger vertical velocity. Their model, however, does not reach a steady state and usually turns into downdraft in later stages even with a tilting angle as large as 45 degrees. Also, although the outgoing rain flux from the tilted cloud was explicitly calculated in their model, the response of the cloud environment to the falling rain was not included.

Cheng (1989a) presented a combined updraft–downdraft spectral cumulus ensemble model that includes the mass, rainwater, and vertical momentum budget equations for both updrafts and downdrafts. The model assumes that the rainwater generated in an updraft falls partly inside and partly outside of the updraft. One of the unique aspects of this model is that the mean tilting angle of the updraft is estimated to determine this partition. It is done by assuming statistically steady states with random perturbations on the cloud-scale horizontal velocity. The vertical velocity and thermodynamic properties of the associated downdrafts are then calculated considering the effects of rainwater loading and evaporation. This model has been applied to diagnostic studies on the effects of convective downdrafts and associated mesoscale processes (Cheng 1989b; Cheng and Yanai 1989). The model has also been incorporated into the A–S cumulus parameterization, and results from semiprognostic tests and GCM experiments are presented by Cheng and Arakawa (1990, 1991a).

Cheng's tilting updraft model in its original form, however, does not allow the detrainment of rainwater through cloud top. This is due to the use of a simplified form of the vertical momentum equation, in which w^2 is locally related to the sum of the thermal buoyancy and rain-drag terms. This relation requires that the rain-drag term be zero (so that the rainwater mixing ratio will be zero) where the thermal buoyancy is zero, leading to a fixed upper boundary condition for the rainwater budget equation. Naturally, this upper boundary condition is inappropriate when in-cloud rain flux is upward at cloud top. The rainwater detraining from cloud top, however, can be an important source for anvil precipitation in a mesoscale convective system. Moreover, not allowing rainwater detrainment at cloud top can significantly distort the overall solutions of the rainwater budget equation. Cheng and Arakawa (1991b; see also the appendix of Arakawa and Cheng 1993) improved Cheng's original model through implementing a more complete form of the vertical momentum equation and a more appropriate upper boundary condition for the rainwater budget equation. In the improved model, the updraft tilting angle is determined through stability of stationary solutions of the coupled rainwater budget and vertical momentum equations. Recently, this procedure of determining the tilting angle was drastically simplified (Cheng and Arakawa 1994), as we discuss in section 8 in more detail.

This paper describes our work on further revisions of the coupled updraft–downdraft model. Section 2 describes the procedures for determining the updraft properties, in particular the vertical distribution of rain water. Section 3 first describes the procedure for finding stationary solutions of the coupled rainwater budget and vertical momentum equations with examples. Two types of solutions are then identified: *solutions for small tilting angles*, which are unstable, and *solutions for large tilting angles*, which are stable. The cause of the instability is interpreted, and the motivation for an optimum choice of the updraft tilting angle for use in cumulus parameterization is explained. Section 4 presents the downdraft model and describes how the model treats entrainment and detrainment for downdrafts. Section 5 looks into the possibility of generalizing the definition of

cloud work function due to the explicit inclusion of rain drag and downdrafts. Sections 6 and 7 present the results of semiprognostic and single-column prognostic tests of the revised A–S cumulus parameterization in which the updraft–downdraft model is implemented. Section 8 presents an updraft model with a simplified rainwater budget equation, which is used in our current applications of the revised A–S parameterization. Finally, section 9 presents a summary and conclusions.

2. Determination of the updraft properties

As in the standard application of the A–S cumulus parameterization, updrafts are classified into subensembles according to the vanishing buoyancy level. For each subensemble thus classified, we define the *fractional rate of entrainment* by

$$\lambda \equiv \frac{1}{m}\frac{\partial m}{\partial z} = \frac{1}{\eta}\frac{\partial \eta}{\partial z}, \tag{2.1}$$

where m is the subensemble updraft mass flux, η is the normalized subensemble updraft mass flux defined by

$$\eta \equiv \frac{m}{m_B}, \tag{2.2}$$

and m_B is the subensemble updraft mass flux at cloud base. In determining the vertical profile of η, we may assume that λ is constant in height, as in the original A–S parameterization, or the rate of entrainment itself given by $\mu \equiv \partial m/\partial z$ is constant in height, as in Moorthi and Suarez (1992) and Cheng and Arakawa (1993). In either case, it is assumed that the vertical profile of the subensemble vertical mass flux is determined by a single scalar parameter, λ or μ in the examples given above. It is further assumed that the thermodynamic properties of the updraft at cloud base are equal to those averaged vertically over the entire subcloud layer. Then, using the moist static energy and water (water vapor plus cloud liquid water) budget equations, with parameterized rainwater generation, and using the saturation assumption for cloud air, we can determine the thermodynamic properties of the updrafts, including the thermal buoyancy and the cloud water mixing ratio, as functions of λ or μ and height. Application of the vanishing-buoyancy condition to cloud top thus determines λ or μ for each subensemble. In this way, the thermodynamic properties of the updrafts and the rate of rainwater generation per unit cloud-base mass flux can be determined for each subensemble as functions of height. For more detailed computational procedures for these steps, see Cheng and Arakawa (1997).

The updraft–downdraft model introduces the rainwater budget equation of the form

$$\frac{\partial}{\partial t}(\rho\sigma q_r) = G - \cos\theta\frac{\partial H}{\partial z}, \tag{2.3}$$

where

$$G \equiv mC_0\ell - \frac{2}{\pi a}\rho\sigma q_r V_t \sin\theta, \tag{2.4}$$

$$H \equiv \rho\sigma q_r(w/\cos\theta - V_t\cos\theta), \tag{2.5}$$

$$\rho\sigma = \frac{m}{w}; \tag{2.6}$$

ρ is the air density, σ is the fractional horizontal area covered by the updraft, q_r is the rainwater mixing ratio in the updraft, C_0 is the coefficient for autoconversion from cloud water to rainwater, ℓ is the cloud water mixing ratio, and θ is the updraft tilting angle. This particular form of the rainwater budget equation is derived for a cylindrical updraft (see Cheng 1989a). The diameter of the cylinder, a, which matters only in the second term on the rhs of (2.4), is treated as a constant for each subensemble and is estimated from $a = 0.2/(\lambda \text{ or } \mu)$. The term G is the net generation of rainwater due to the autoconversion of cloud water minus the loss of rainwater through the outgoing rain flux, while H is the in-cloud rain flux (upward positive). Raindrops are assumed to fall with the terminal velocity V_t relative to the updraft vertical velocity w. Following Soong and Ogura (1973), the mean terminal fall velocity of raindrops is calculated from

$$V_t = 36.34(\rho q_r)^{0.1364}(\rho/\rho_0)^{-0.5} \text{ m s}^{-1}, \tag{2.7}$$

where ρ_0 is a reference air density.

To calculate the vertical distribution of q_r for each subensemble, we use the stationary version of (2.3). Omitting the time derivative term in (2.3), using (2.4), (2.5), (2.6), and (2.2) in the result, and assuming that θ is independent of height,

$$0 = \eta C_0\ell - \frac{2}{\pi a}\frac{\eta}{w}q_r V_t\sin\theta - \frac{\partial}{\partial z}\left\{\frac{\eta}{w}q_r(w - V_t\cos^2\theta)\right\}. \tag{2.8}$$

Equation (2.8) involves the updraft vertical velocity w. To calculate w, we use the vertical momentum equation given by

$$\frac{\partial}{\partial z}(mw) = \rho\sigma\frac{B - gq_r}{1 + \gamma^*}, \tag{2.9}$$

where B is the thermal buoyancy, including the loading of cloud water; g is the gravitational acceleration; and γ^* is the virtual mass coefficient (Simpson and Wiggert 1969). Using (2.6) and (2.2), (2.9) can be rewritten as

$$\frac{\partial}{\partial z}(\eta w)^2 = 2\eta^2\frac{B - gq_r}{1 + \gamma^*}. \tag{2.10}$$

Integrating (2.10) from cloud base to a height z, we obtain

$$(\eta w)^2 = w_B^2 + \int_{z_B}^{z}\frac{2\eta^2}{1 + \gamma^*}(B - gq_r)\,dz, \tag{2.11}$$

where the subscript B denotes cloud base.

As mentioned earlier, we specify the vertical profile of η for each subensemble. The thermal buoyancy can then be calculated using the moist static energy and water-vapor budget equations applied to each subensemble. Using the thermal buoyancy B thus obtained, the vertical velocity can be obtained from (2.11) if the vertical profile of q_r is known. In practice, however, we must solve (2.8) and (2.11) simultaneously. As we discuss later, the coupling of these two equations due to the rain-drag term in (2.11) has a crucial role in determining the solutions of these equations.

3. Solution of the stationary rainwater budget and vertical momentum equations

For numerical solution of the coupled rainwater budget and vertical momentum equations, (2.8) and (2.11) must be discretized. Let us identify the model layers by an integer index $k = 1, 2, 3, \ldots, N$ (increasing downward) and levels that separate the adjacent model layers by half-integer indices such as $k - 1/2$, $k + 1/2$, etc. Layer N represents the planetary boundary layer (PBL) of the model. Cloud base is assumed to be at the PBL top (level $N - 1/2$). We define all cloud variables at half-integer levels except those at cloud top, which is chosen to be at an integer level. For details of the discretization and discussion of associated problems, see Cheng and Arakawa (1996).

Let D_k for $N \geq k \geq i$ be the rhs of the discrete version of the rainwater budget equation (2.8). For a given vertical profile of q_r, D_k can be calculated for all k. To find q_r satisfying $D_k = 0$ by iteration, we linearize the set of $N - i + 1$ equations with respect to q_r', where q_r' is the deviation of q_r from the given vertical profile. The result can be written in a matrix form as

$$0 = \mathbf{D} + \mathbf{C}\,\mathbf{q}_r', \tag{3.1}$$

where $\mathbf{D}$ and $\mathbf{q}_r'$ are column vectors consisting of D_k and $(q_r')_{j-1/2}$ for $N \geq k \geq i$ and $N \geq j \geq i$, and $\mathbf{C}$ is an $N - i + 1$ by $N - i + 1$ matrix given by

$$C_{k,j} = \begin{cases} \dfrac{\partial D_k}{\partial (q_r')_{j-1/2}} & \text{for } N \geq k \geq i \text{ and } N \geq j \geq k \\ 0, & \text{otherwise.} \end{cases} \tag{3.2}$$

After solving (3.1) for $\mathbf{q}_r'$, the result is added to the given profile of $\mathbf{q}_r$ to obtain a new profile. The vertical velocity w is then updated using the discrete version of the vertical momentum equation (2.11). (We have found that the overall solution is not sensitive to the choice of w at cloud base, w_B, if it is finite. Currently, we are using $w_B = 0.1$ m s^{-1}.) Also, the elements of $\mathbf{D}$ and $\mathbf{C}$ are updated. This procedure is repeated until it converges.

Let us assume, for the time being, that the tilting angle of the updraft, θ, is known. Figure 1 shows an example of the solutions of the coupled system for a prescribed θ ranging from 0° to 50°. This example is for a particular cloud type reaching the 16-mb level calculated using the Global Atmospheric Research Program (GARP) Atlantic Tropical Experiment (GATE) Phase III mean data (see Cheng 1989b) as input. In the figure we see that the vertical profiles of rainwater mixing ratio, vertical velocity, in-cloud rain flux, and outgoing rain flux change smoothly as θ increases from 0° to 22° and from 25° to 50° with a gap between 22° and 25°. Within this gap, the iteration described above fails to converge and, consequently, stationary solutions cannot be found. For convenience, we call the two types of solutions separated by the gap *solutions for small tilting angles* (0°–22° in this case) and *solutions for large tilting angles* (25°–50° in this case), respectively.

For very small values of θ, the in-cloud rain flux is dominantly downward, so that $q_r \approx 0$ holds near cloud top. The outgoing rain flux, which depends on $\sin\theta$ [see the second term on the rhs of (2.8)], is small for those angles, so that the divergence of in-cloud rain flux should approximately balance the generation term in the rainwater budget equation. As θ increases, however, $w - V_t\cos^2\theta$ changes its sign and the in-cloud rain flux becomes upward with its maximum at an upper level (at 300–400 mb in this case; see Fig. 1c) with strong convergence above. This convergence, plus the generation, must be balanced by the outgoing rain flux. To have a sufficiently large amount of the outgoing rain flux to maintain this balance, however, a large value of q_r is required (see Fig. 1a). It is then reasonable that this type of balance fails to exist when θ is larger than a critical value (about 22° in this case), because the required value of q_r is too large.

For θ larger than the critical value, the iteration converges to *solutions for large tilting angles*, which represents a different type of balance. Compared to *solutions for small tilting angles*, these solutions are characterized by relatively small upper-level rainwater mixing ratios approximately uniform in height near cloud top (see Fig. 1a), by relatively large vertical velocities at upper levels including cloud top (see Fig. 1b), by dominantly upward in-cloud rain fluxes extending to cloud top (see Fig. 1c), and by approximately θ-independent outgoing rain fluxes (see Fig. 1d). The large upward upper-level in-cloud rain fluxes mean large detrainment of rainwater near cloud top. At $\theta = 25°$ in this case, the detrainment of rainwater from cloud top accounts for about 41% of the total rainwater generated in the updraft. This ratio increases as the tilting angle increases. In contrast, this ratio for the solutions for small tilting angles is less than 3%.

For small tilting angles, the upper-level rainwater mixing ratio increases as θ increases, while the upper-level vertical velocity decreases. For large tilting angles, on the other hand, the upper-level rainwater mixing ratio decreases as θ increases, while the upper-level vertical velocity increases. These changes are consistent in view of the drag effect in the vertical momentum equation. An extension of the solutions for large tilting angles

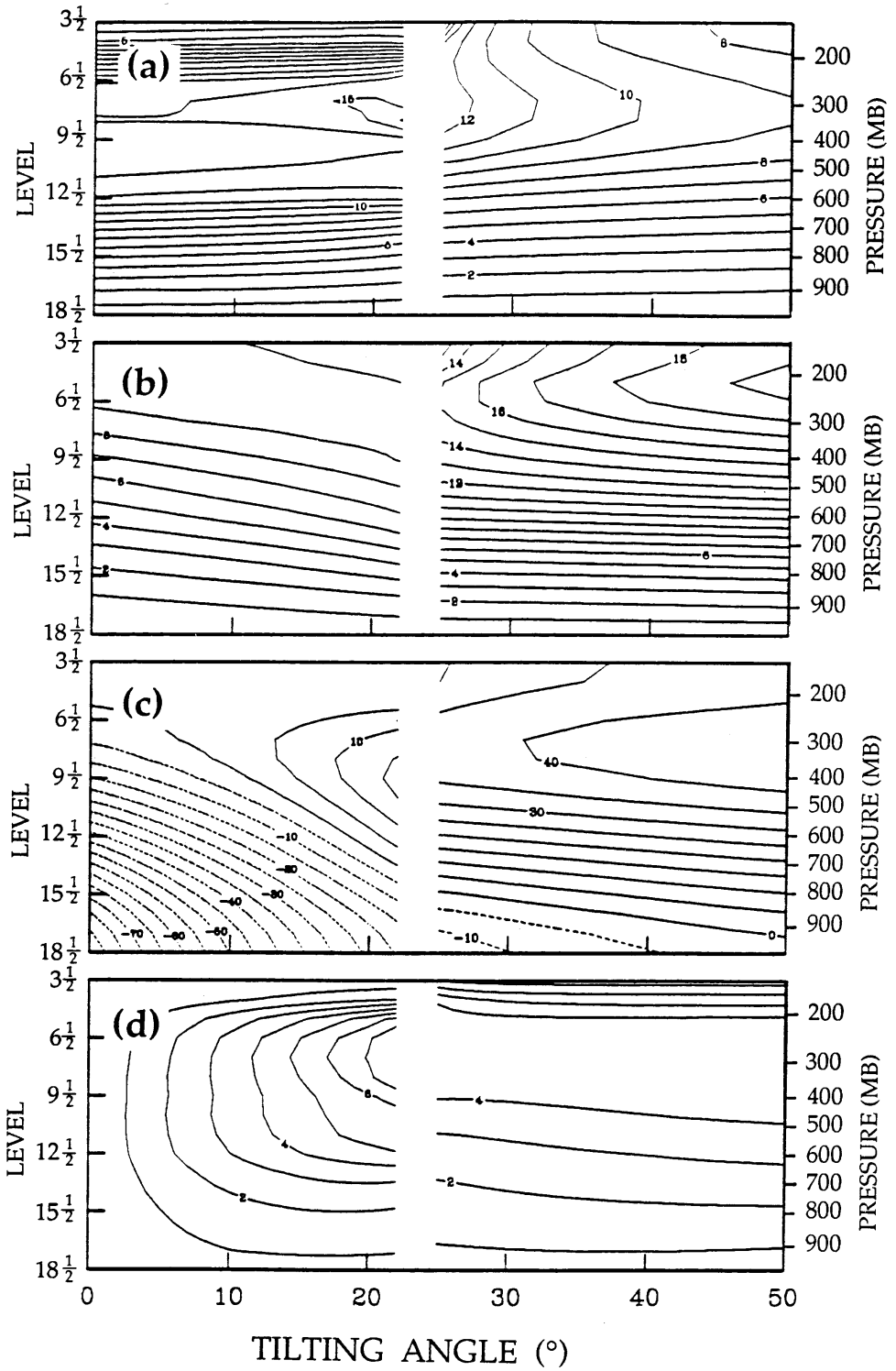

FIG. 1. Solutions of the coupled rainwater budget and vertical momentum equations for a range of prescribed θ for clouds reaching the 160-mb level calculated using the GATE Phase III mean data as input: (a) rainwater mixing ratio (g kg^{-1}), (b) vertical velocity (m s^{-1}), (c) in-cloud, and (d) outgoing rain flux (arbitrary unit). The vertical coordinate is shown using the half-integer index defined in section 3 with $N = 19$ (left) and pressure (right).

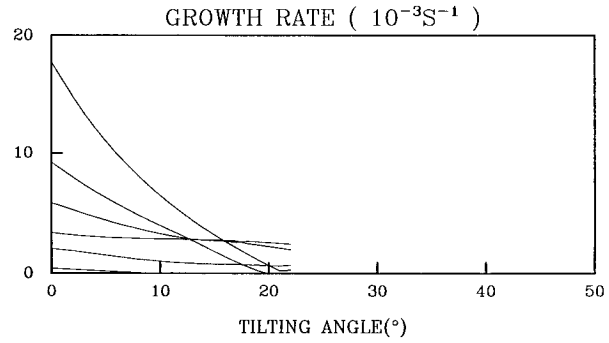

FIG. 2. Growth rate of perturbed rainwater mixing ratio superposed on the stationary solutions shown in Fig. 1.

may exist for θ smaller than the critical value, in addition to the solutions for small tilting angles. In practice, however, we have not found more than one solution for a given value of θ.

Next we examine the stability of these stationary solutions with respect to a perturbation on the vertical distribution of rainwater. For this purpose, we restore the time derivative term in the left-hand side of the rainwater budget equation (3.1) while keeping the vertical momentum equation in the diagnostic form given by (2.11). Here we assume that the timescale of dynamical adjustment, which adjusts the vertical momentum toward a balance, is much shorter than that of establishing an equilibrium for the rainwater distribution. After linearization, our problem then reduces to the problem of finding eigenvalues of the matrix **C** defined in (3.2). Figure 2 shows that the real part of the eigenvalues are positive in the range of θ from 0° to 22° and are practically zero for larger values of θ. Comparing Fig. 2 to Fig. 1, we thus see that the *solutions for small tilting angles* are unstable, while the solutions for large tilting angles are stable. The existence of instability for small tilting angles was confirmed through time integrations with various initial conditions (Cheng and Arakawa 1991b).

The instability of the solutions for small tilting angles is through a positive feedback in the coupling of the rainwater budget and vertical momentum equations, which includes the rain-drag term in the latter. For simplicity, let us first consider the case with $\theta = 0$. Suppose that q_r is positively perturbed locally at a certain level. Due to the larger deceleration of the updraft by the increased rain drag there, the upward air velocity immediately above that level becomes weaker. This produces an accumulation of rainwater at the level of the q_r perturbation. This produces a positive feedback. Figure 3 illustrates this situation when $w = V_t$ for the unperturbed state. As the updraft tilting angle θ increases, however, the stabilizing effect due to the outgoing rain flux becomes significant.

A simple analysis given below can illustrate the existence of instability. Using $\lambda = 0$, $\eta = 1$, and $\rho\sigma = m/w = m_B\eta/w = m_B/w$, the vertical momentum equation (2.9) and the rainwater budget equation (2.8), with the time derivative term restored, may be written as

$$w\frac{\partial w}{\partial z} = \frac{B - gq_r}{1 + \gamma^*}, \tag{3.3}$$

$$\frac{\partial}{\partial t}\left(\frac{q_r}{w}\right) = C_0\ell - \frac{2}{\pi a}\frac{q_r}{w}V_t\sin\theta - \frac{\partial}{\partial z}\left\{\frac{q_r}{w}(w - V_t\cos^2\theta)\right\}. \tag{3.4}$$

Consider a basic state with $w = W$ and $q_r = Q_r$, where W and Q_r are constant. Assume $(q_r/w)' \approx q_r'/W$ and V_t is a constant. Linearizing (3.3) and (3.4),

$$W\frac{\partial w'}{\partial z} = -\frac{g}{1 + \gamma^*}q_r' \tag{3.5}$$

and

$$\frac{\partial q_r'}{\partial t} = -\frac{2}{\pi a}q_r'V_t\sin\theta - \frac{\partial q_r'}{\partial z}(W - V_t\cos^2\theta) - Q_r\frac{\partial w'}{\partial z}. \tag{3.6}$$

The first term on the rhs of (3.6) represents a damping effect. The second term is the advection term, which is responsible for the imaginary part of the eigenvalue. Using (3.5), the third term may be written as

$$-Q_r\frac{\partial w'}{\partial z} = \frac{g}{1 + \gamma^*}\frac{Q_r}{W}q_r'. \tag{3.7}$$

Combining this with the first term, we may rewrite (3.6) as

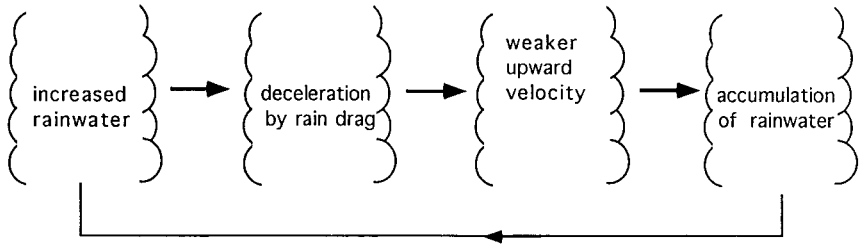

FIG. 3. An illustration of the instability in the vertical distribution of rainwater mixing ratio when $w = V_t$ for the unperturbed state.

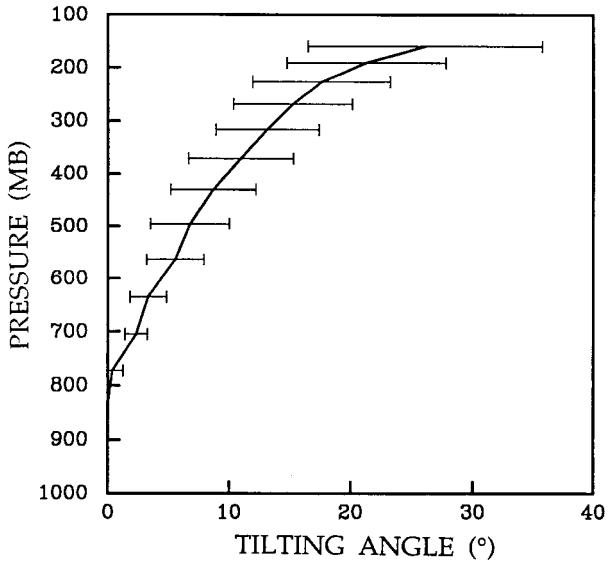

FIG. 4. The time-averaged tilting angles and their standard deviations as functions of cloud type identified by the pressure at cloud top for the GATE Phase III period.

$$\frac{\partial q_r'}{\partial t} = -\frac{\partial q_r'}{\partial z}(W - V_t\cos^2\theta) + \left[-\frac{2}{\pi a}V_t\sin\theta + \frac{g}{1+\gamma^*}\frac{Q_r}{W}\right]q_r'. \quad (3.8)$$

The quantity inside the brackets is positive when Q_r/W $\sin\theta$ is larger than a critical value, indicating a growth. Thus an untilted updraft is unconditionally unstable. The *solutions for large tilting angles* are stable because q_r is smaller and both w and θ are larger compared to the solutions for small tilting angles.

So far we have treated the updraft tilting angle, θ, as a given constant. In principle, we cannot determine θ uniquely with our model, which is not closed because it does not use the convective-scale horizontal momentum equation. We must, however, at least choose one of the two types of solutions described above because their vertical structures are quite different. One of the stable solutions, that is, one of the solutions for large tilting angles, seems to be a natural choice for the present purpose. Then we proceed in the model as follows. For a range of θ, we solve the stationary rainwater budget and vertical momentum equations and examine stability of the solutions. We then choose an angle, θ, in the stable range. As far as θ is in that range, the precise choice of θ does not seem to be very important since the solutions for large tilting angles do not show much θ dependence of the outgoing rain flux, which is the rain flux available for the downdraft. In practice, we choose the smallest tilting angle in the stable range since processes that may favor larger tilting angles are not included in the model. Figure 4 shows the time-averaged tilting angles determined in this way and their standard deviations as functions of cloud type identified by the pressure at cloud top for the GATE Phase III period. We see that the tilting angle can vary by a factor of 2 even for the same cloud type at the same location.

It should be noted that the model does not attempt to determine the direction of updraft tilting. The direction should depend on horizontal asymmetries such as the vertical shear of horizontal wind. Without such asymmetries, the direction should depend on unknown initial conditions and, therefore, it may have to be treated as a consequence of stochastic processes. What we attempt to do in the model is to narrow down the range of possible tilting angles for use in cumulus parameterization. As long as we are primarily interested in the thermodynamical effects of cumulus convection, our choice seems to be reasonable, at least for normal situations.

The procedure for determining the updraft properties described in this section has recently been greatly simplified (Cheng and Arakawa 1994) as described in section 8 in more detail.

4. The downdraft model

After we determine the updraft tilting angle for each subensemble, a downdraft model is used to find properties of the associated downdraft. In the model, downdrafts are assumed to be initiated and maintained by the loading and evaporation cooling of rainwater. With the known rain flux from updrafts, the thermodynamic properties, vertical velocity, and mass flux of downdrafts are obtained by solving the equations given in this section. In these equations, z increases downward, with a positive w representing downward motion, and all variables refer to downdrafts unless otherwise mentioned.

The downdraft model consists of the budgets of mass, water vapor, moist static energy, total water, and vertical momentum for each subensemble. It includes evaporation of rainwater, entrainment from the environment, and detrainment into the environment. Conservation of mass and moist static energy can be expressed as

$$\frac{\partial m}{\partial z} = \varepsilon - \delta, \quad (4.1)$$

$$\frac{\partial mh}{\partial z} = \varepsilon\bar{h} - \delta h, \quad (4.2)$$

where m is the downdraft mass flux, ε is the rate of mass entrainment per unit height, δ is the rate of mass detrainment per unit height, and h and h are the moist static energy of the environment and the downdraft respectively.

Similarly, the water vapor budget equation may be expressed as

$$\frac{\partial mq}{\partial z} = \varepsilon\bar{q} - \delta q + E_r, \quad (4.3)$$

where $\bar{q}$ and q are the water vapor mixing ratios of the

environment and the downdraft, respectively, and E_r is the source of water vapor due to the evaporation of rainwater. Following Ogura and Takahashi (1971), we use the expression

$$E_r = \sigma \frac{(1 - q/q^*)C(\rho q_r)^{0.525}}{5.4 \times 10^5 + 2.55 \times 10^6/(pq^*)}, \quad (4.4)$$

where $\sigma \equiv m/\rho w$ is the fractional horizontal area covered by the downdraft, w is the vertical velocity of the downdraft, q_r is the rainwater mixing ratio of the downdraft, q^* is the saturation water vapor mixing ratio, p is the pressure, and C is the ventilation coefficient given by

$$C = 1.6 + 124.9(\rho q_r)^{0.2046}. \quad (4.5)$$

The vertical momentum equation we use is similar to (2.9). It may be written as

$$\frac{\partial mw}{\partial z} = -\rho\sigma \frac{B - gq_r}{1 + \gamma^*} - \delta w, \quad (4.6)$$

where B is the thermal buoyancy. [Recall that z here is positive downward.]

The budget of rainwater is determined by

$$\frac{\partial P_d}{\partial z} = m_B R_A - E_r, \quad (4.7)$$

where P_d is the rain flux within the downdraft given by

$$P_d \equiv \rho\sigma q_r(w + V_t), \quad (4.8)$$

R_A is the rain flux from the updraft to the downdraft per unit height per unit m_B, and m_B is the updraft mass flux at cloud base. From the second term on the rhs of (2.4), we see that

$$m_B R_A \equiv \left(\frac{2}{\pi a}\rho\sigma q_r V_t \sin\theta\right)_u, \quad (4.9)$$

where the subscript u refers to the updraft.

We now consider the problem of formulating the vertical change of downdraft mass flux, m. First, differentiating $m = \rho\sigma w$ with respect to z,

$$\frac{1}{m}\frac{\partial m}{\partial z} = \frac{1}{\sigma}\frac{\partial \sigma}{\partial z} + \frac{1}{\rho w}\frac{\partial(\rho w)}{\partial z}. \quad (4.10)$$

We then assume that σ is equal to the fractional horizontal area covered by the rainfall outside the updraft. Processes that can change this area with height are the increase of the area due to the tilt of the updraft, the decrease of the area due to the horizontal convergence of falling raindrops, and the decrease of the rain-covered area due to evaporation of raindrops along the edge of the downdraft. Accordingly, we can express

$$\frac{\partial \sigma}{\partial z} = \left(\frac{\partial \sigma}{\partial z}\right)_{\text{tilt}} + \left(\frac{\partial \sigma}{\partial z}\right)_{\text{conv}} + \left(\frac{\partial \sigma}{\partial z}\right)_{\text{evap}}. \quad (4.11)$$

To express the first term on the rhs of (4.11), we consider a cylindrical updraft as we did in deriving (2.3). For a tilted cylinder with radius a and tilting angle θ, the horizontally projected area of the cylinder increases downward by $2a\tan\theta$ per unit height. On the other hand, the number of cylinders in the horizontal area σ is given by $\sigma\cos\theta/\pi a^2$. Then the downward increase of the rain-covered area due to the vertical tilt of the updraft can be expressed as

$$\left(\frac{\partial \sigma}{\partial z}\right)_{\text{tilt}} = [(2a\tan\theta)(\sigma\cos\theta/\pi a^2)]_u = \left[\frac{2}{\rho\pi a}\frac{m}{w}\sin\theta\right]_u. \quad (4.12)$$

Here $\sigma = m/(\rho w)$ has been used.

To express the second term on the rhs of (4.11), we ignore rain evaporation, whose effect is represented by the third term. Let us first consider the vertical change of σ due to the horizontal convergence of raindrops with no terminal velocity. For this hypothetical situation, raindrops and the surrounding air move together; hence there is neither entrainment nor detrainment. Then, from (4.10) and (4.11), $(\partial\sigma/\partial z)_{\text{conv}}$ becomes

$$\left[\left(\frac{\partial \sigma}{\partial z}\right)_{\text{conv}}\right]^* \equiv -\left\{\frac{\sigma}{\rho w}\frac{\partial \rho w}{\partial z} + \left(\frac{\partial \sigma}{\partial z}\right)_{\text{tilt}}\right\}. \quad (4.13)$$

We next relate the value of $(\partial\sigma/\partial z)_{\text{conv}}$ with nonzero terminal velocity to $[(\partial\sigma/\partial z)_{\text{conv}}]^*$. Assuming stationarity for the downdraft, we can express the ratio between $(\partial\sigma/\partial z)_{\text{conv}}$ and $[(\partial\sigma/\partial z)_{\text{conv}}]^*$ by the ratio between the downward air velocity at the edge of the downdraft and that of raindrops. Then

$$\left(\frac{\partial \sigma}{\partial z}\right)_{\text{conv}} \Bigg/ \left[\left(\frac{\partial \sigma}{\partial z}\right)_{\text{conv}}\right]^* = w/(w + V_t). \quad (4.14)$$

From (4.13) and (4.14), we obtain

$$\left(\frac{\partial \sigma}{\partial z}\right)_{\text{conv}} = -\frac{w}{w + V_t}\left\{\frac{\sigma}{\rho w}\frac{\partial \rho w}{\partial z} + \left(\frac{\partial \sigma}{\partial z}\right)_{\text{tilt}}\right\}. \quad (4.15)$$

We note that substitution of (4.11) into (4.10) and use of (4.15) give

$$\frac{1}{m}\frac{\partial m}{\partial z} = \frac{1}{\sigma}\left(\frac{\partial \sigma}{\partial z}\right)_{\text{evap}} - \frac{V_t}{w}\frac{1}{\sigma}\left(\frac{\partial \sigma}{\partial z}\right)_{\text{conv}}. \quad (4.16)$$

Thus, two effects can produce the (net) entrainment: one is the evaporation of raindrops around the edge of the downdraft and the other is the convergence of raindrops due to nonzero V_t.

Finally, we assume that evaporation of raindrops effectively takes place along the edge of the downdraft. Then the fractional rate of the vertical change of σ due to evaporation is given by

$$\frac{1}{\sigma}\left(\frac{\partial \sigma}{\partial z}\right)_{\text{evap}} = -\frac{E_r}{P_d}, \quad (4.17)$$

where P_d is the rain flux within the downdraft defined by (4.8).

It remains to formulate the rates of entrainment and detrainment, ε and δ in (4.1)–(4.3) and (4.6). There is a notable difference between updrafts and downdrafts regarding the role of entrainment. Unlike updrafts, downdrafts may originate above the layer of conditional instability due to the drag by rainfall. It is difficult for downdrafts to gain significant downward buoyancy under this situation, unless the unsaturated environmental air is entrained into the downdraft to produce evaporation cooling. In this way, even a small amount of entrainment can be important for initiating downdrafts. Here what matters is the actual entrainment, ε, rather than the net entrainment, $\varepsilon - \delta$, and their difference may not be negligible when ε is small.

Here we only consider the entrainment due to horizontal confluence. We first note that the mean inward component of the cloud-scale velocity near the downdraft edge is given by

$$\bar{u} \equiv \frac{1}{\rho L_d}\left(\frac{\partial m}{\partial z}\right)_{\text{conv}}, \tag{4.18}$$

where L_d is the length of the interface between the downdraft and the cloud environment on a horizontal cross section. Note that, from (4.16),

$$\left(\frac{\partial m}{\partial z}\right)_{\text{conv}} = -\frac{V_t}{w}\frac{m}{\sigma}\left(\frac{\partial \sigma}{\partial z}\right)_{\text{conv}}. \tag{4.19}$$

We then consider perturbation of cloud-scale horizontal velocity whose component into the downdraft is u'. The sign of u' is defined to be positive (negative) if the perturbed motion is inward (outward). Then $\bar{u} + u' > 0$ means that the air is entraining into the downdraft, while $\bar{u} + u' < 0$ means that the air is detraining from the downdraft. It is then possible to formulate expected values of ε and δ if we know the probability distribution of u'. The appendix gives an example of such formulation, which is used in the current version of the model.

Discretization of the downdraft equations and their solving procedures are described in Cheng and Arakawa (1997).

5. Components of the cloud work function

As in the original A–S parameterization, we now introduce the cloud work function (CWF) quasi-equilibrium assumption for the primary closure. In general, the thermal buoyancy of updrafts is the main force for generation of cloud kinetic energy. The A–S parameterization thus defines CWF as the work done by the thermal buoyancy of the updraft per unit updraft mass flux at cloud base. Lord and Arakawa (1980) consider the effects of rainwater loading as a part of the mechanisms for dissipation of cloud kinetic energy. In the present combined updraft–downdraft model, the thermal buoyancy and rainwater drag are explicitly calculated for both the updraft and associated downdraft. We may, therefore, redefine CWF as the work done by the net buoyancy, the sum of the thermal buoyancy and the rainwater drag, of the updraft per unit updraft mass flux at cloud base. We may also include the generation of cloud kinetic energy due to the downdraft in the definition of CWF.

Let B_u, D_u, B_d, and D_d be the thermal buoyancy of the updraft, the rainwater drag on the updraft, the thermal buoyancy of the downdraft, and the rainwater drag of the downdraft, respectively. Arakawa–Schubert define CWF by

$$A_1 \equiv \int_{z_B}^{z_T} \eta_u B_u \, dz, \tag{5.1}$$

where η_u is the updraft mass flux normalized by its cloud base value, and z_T and z_B are the heights of cloud top and cloud base, respectively. Lord and Arakawa (1980) presented the statistics of A_1 for a variety of observed situations.

As mentioned above, we may redefine CWF by

$$A_2 \equiv \int_{z_B}^{z_T} \eta_u (B_u + D_u) \, dz \tag{5.2}$$

or by

$$A_3 \equiv \textstyle\int_{z_B}^{z_T} \{\eta_u (B_u + D_u) + \eta_d (B_d + D_d)\} \, dz, \tag{5.3}$$

where η_d is the downdraft mass flux normalized by the updraft mass flux at cloud base.

Figure 5 shows A_1, A_2, and A_3 for clouds with top at 190 mb calculated for the GATE Phase III period. In general, A_2 is only about one-third of A_1, indicating that the rainwater drag offsets about two-thirds of the thermal buoyancy for updraft. The difference between A_3 and A_2 represents the generation of cloud kinetic energy by the net buoyancy of the downdraft, which is a relatively small fraction of A_2. In spite of the differences in their magnitudes, however, A_1, A_2, and A_3 are approximately proportional to each other. Consequently, the quasi-equilibrium of A_2 or A_3 should also mean the quasi-equilibrium of A_1. We therefore continue to use A_1 in implementing the CWF quasi-equilibrium assumption.

6. Semiprognostic tests

As we did with the earlier version (Cheng and Arakawa 1990, 1991a), we have tested the revised A–S cumulus parameterization described in this paper semiprognostically. A semiprognostic test is a one-step prediction of the cumulus activity for a given large-scale condition. The procedure we use for computing the cumulus effects in the test is identical to that in fully prognostic models except that the definition of the large-scale forcing follows Lord (1982) so that the calculation at each observation time is independent from those at other time points.

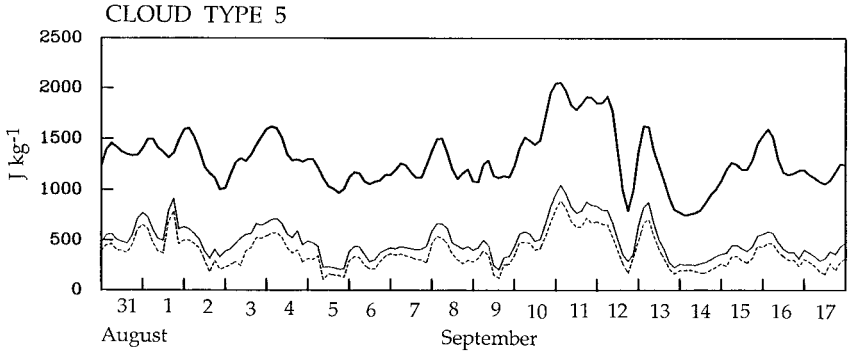

FIG. 5. Cloud work functions A_1 (thick solid line), A_2 (dashed line), and A_3 (thin solid line) defined by (5.1), (5.2), and (5.3), respectively, calculated for clouds with top at 190 mb for the GATE Phase III period.

To verify the results, we use the cumulus effects diagnostically determined from the residuals in the large-scale budget equations applied to a time sequence of observations. The 3-h, 1° × 1° gridded data for GATE Phase III (see Sui et al. 1989; Cheng 1989b), together with radiation heating taken from Cox and Griffith (1978, 1979), are used for this purpose. These data are interpolated to integer levels representing 19 layers. The lowest layer is defined as the PBL. The top of this layer, which is at 969.10 mb, is taken as cloud base. In the tests described below, no clouds penetrate the 146.16-mb level.

Figure 6 shows the time–height sections of diagnostically calculated $Q_{1C} \equiv Q_1 - Q_R$ and Q_2 covering the entire period of GATE Phase III. Here Q_1 and Q_2 are apparent heat source and apparent moisture sink (Yanai et al. 1973), respectively, and Q_R is the radiation heating. In these figures we see that not only the magnitudes but also the heights of local maxima of Q_{1C} and Q_2 fluctuate highly in time. The strong coupling and separation of the peaks of Q_{1C} and Q_2 indicate that Q_{1C} is primarily due to condensation processes associated with cumulus convection.

In the updraft-only model, only the cloud environment above the PBL is modified by clouds, with no feedback through the changes of the PBL properties other than its depth. In the combined updraft–downdraft model, the detrainment from downdrafts can significantly modify the thermodynamic properties of the PBL. To separate the problem of cumulus parameterization from that of a PBL parameterization, however, we performed ''fixed PBL'' experiments, in which all PBL processes are made implicit by fixing the properties of the PBL in calculating the large-scale forcing and mass flux

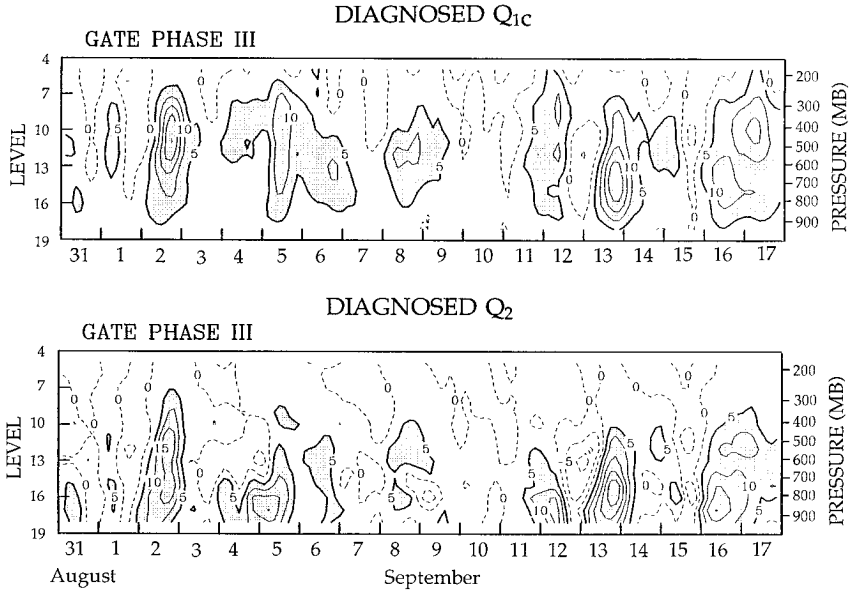

FIG. 6. Time–height sections of diagnostically calculated $Q_{1C} \equiv Q_1 - Q_R$ and Q_2 (divided by c_p) covering GATE Phase III. Unit: K day^{-1}. The vertical coordinate is shown using the integer index defined in section 3 with $N = 19$ (left) and pressure (right).

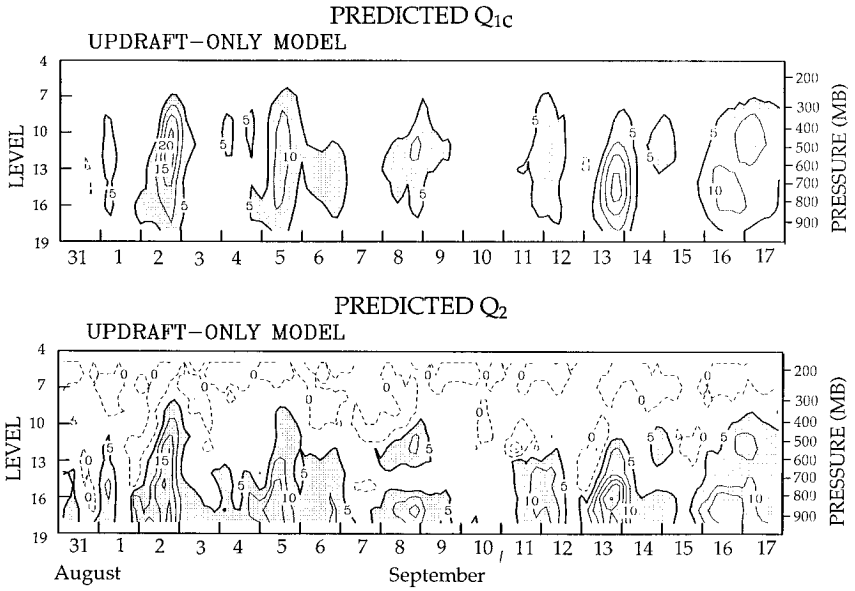

FIG. 7. As in Fig. 6 but semiprognostically calculated with the updraft-only model.

kernel. [For definitions of these quantities, see Lord (1982).]

Time–height sections of Q_{1C} and Q_2 semiprognostically calculated with the updraft-only model are shown in Fig. 7. Comparing Fig. 7 to Fig. 6, we see that the calculated cumulus heating rates by the updraft-only model agree very well with the observation. We also see, however, that the updraft-only model does not predict the cumulus drying rates as well as the cumulus heating rates. Figure 8a shows the vertical profiles of the diagnostically (solid) and semiprognostically (dashed) calculated Q_{1C} and $-Q_2$ averaged in time over the Phase III period. We see that, in the time average, the agreement between the observed and predicted cumulus heating, $Q_{1C} \equiv Q_1 - Q_R$, is excellent, while there is a systematic difference between the observed and predicted cumulus moistening, $-Q_2$. Apparently, the updraft-only model tends to overestimate the cumulus drying effect throughout the entire cloud layer.

Figure 9 shows the time–height sections of Q_{1C} and Q_2 semiprognostically calculated with the updraft–downdraft model. The time averages of these quantities are shown in Fig. 8b. Comparing Fig. 9 with Fig. 7, we see that Q_{1C} and Q_2 predicted with the updraft–down-

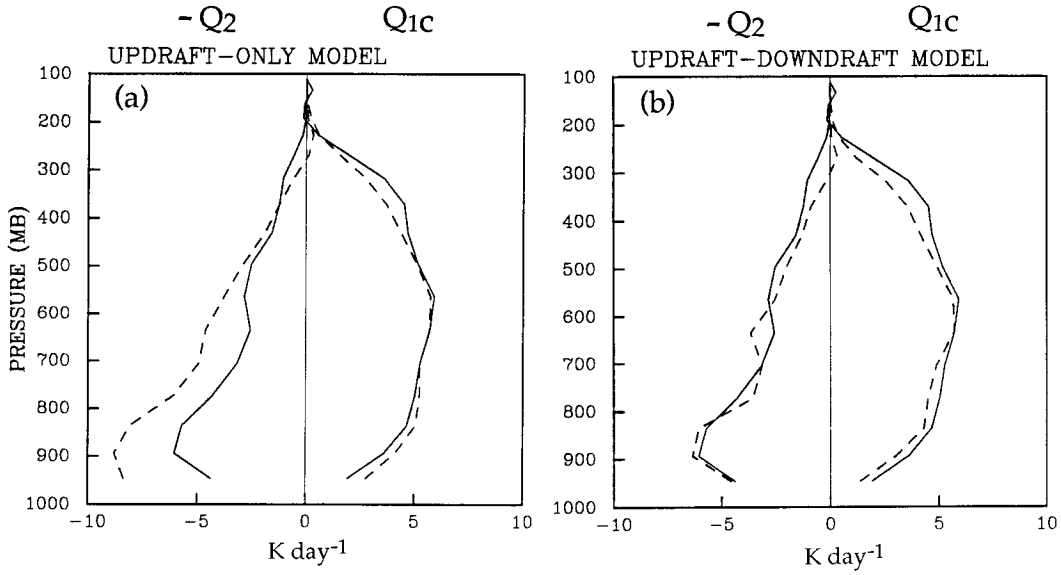

FIG. 8. Time-averaged vertical profiles of the observed (solid) and semiprognostically calculated (dashed) Q_{1C} and $-Q_2$ (a) with the updraft-only model and (b) with the updraft–downdraft model.

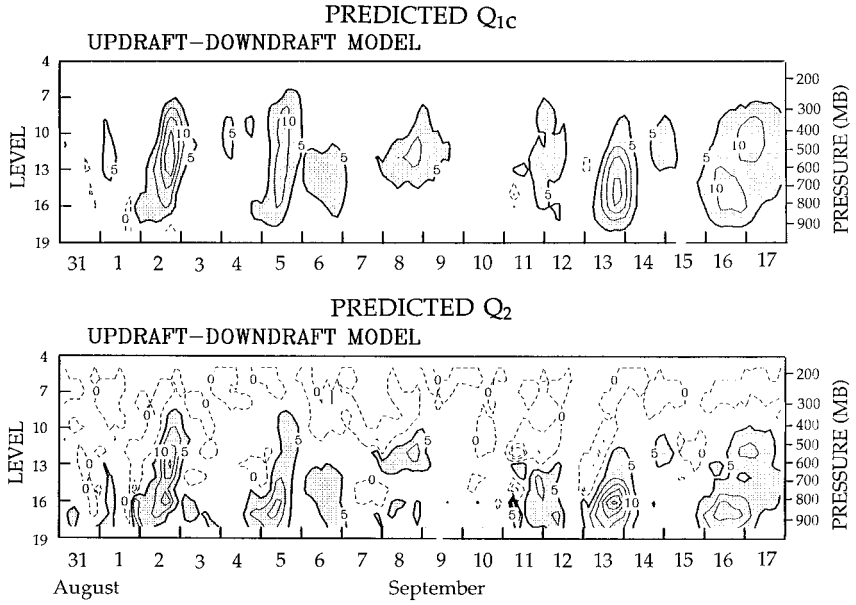

FIG. 9. As in Fig. 6 but semiprognostically calculated with the updraft–downdraft model.

draft model are similar to those predicted by the updraft-only model. Comparing Fig. 8b with Fig. 8a, however, we see that the agreement with the observed values is significantly improved for Q_2 by the inclusion of downdrafts. The excessive cumulus drying predicted by the updraft-only model at lower levels is now almost completely eliminated. Although we cannot show it in the results of this fixed-PBL experiment, we note that the updraft–downdraft model predicts a large amount of drying below cloud base because the downdraft air is usually drier than the environmental air in the subcloud layer. Thus the inclusion of downdrafts shifts a significant portion of cumulus drying downward from the cloud layer to the subcloud layer.

Figure 10 shows the decomposition of the time-averaged (Fig. 10a) cumulus moistening $-Q_2$ and (Fig. 10b) cumulus heating Q_{1C} semiprognostically calculated with the updraft-only model into the subsidence effect (dashed line) and the detrainment effect (chain line). Figure 11 shows similar decomposition but for those

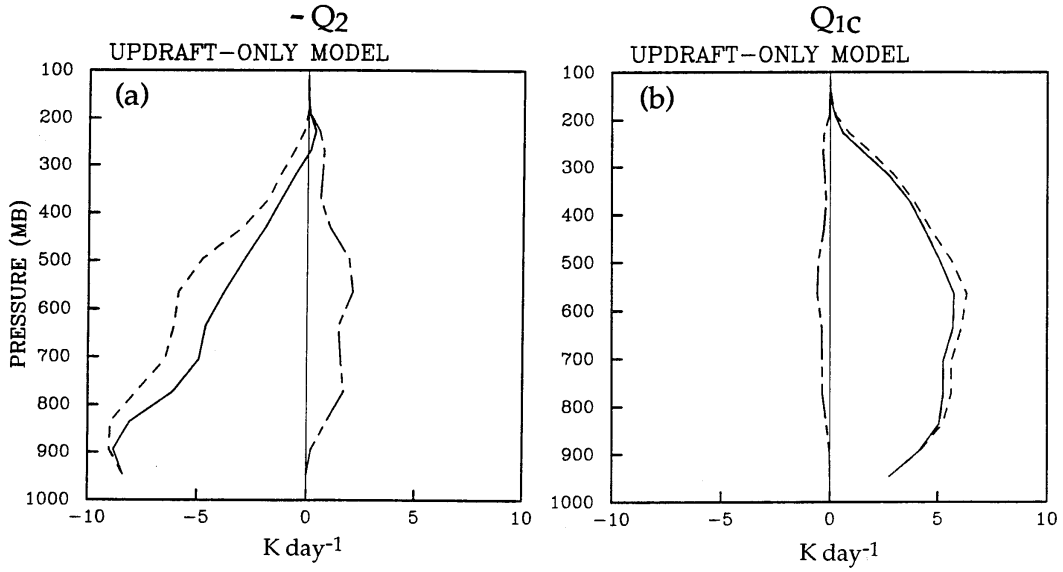

FIG. 10. Decomposition of the time-averaged (a) cumulus moistening $-Q_2$ and (b) cumulus heating Q_{1C} predicted with the updraft-only model into the subsidence effect (dashed line) and the detrainment effect (chain line). The total cumulus effect shown by the dashed line in Fig. 8a is now shown by the solid line.

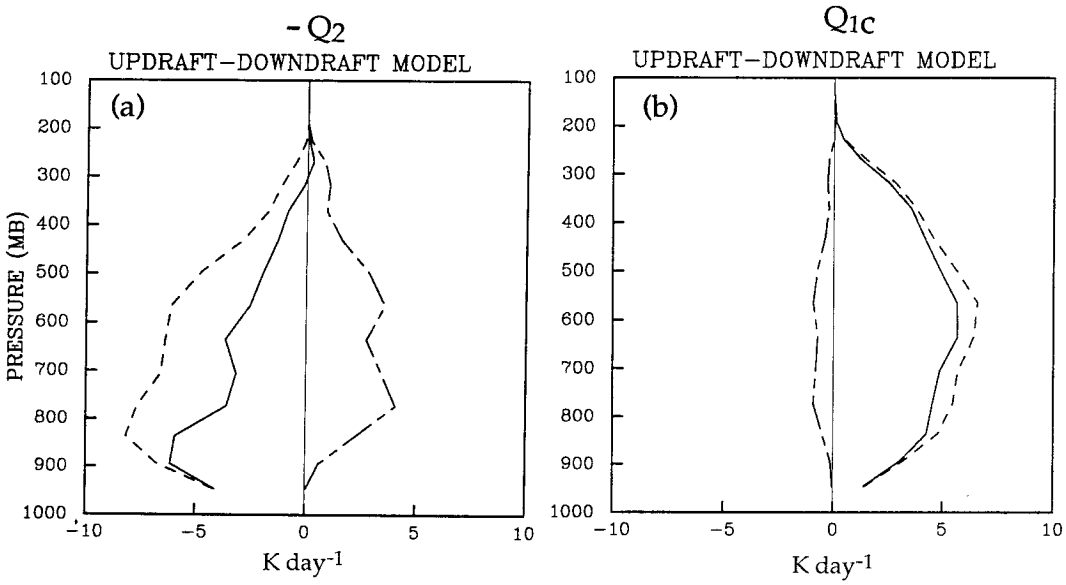

FIG. 11. As in Fig. 10 but for those calculated with the updraft–downdraft model.

calculated with the updraft–downdraft model. It is interesting to see that the reduction of cumulus drying in the cloud layer is not simply through reduction of cumulus subsidence. We see that this effect is confined in a very shallow layer above cloud base centered around 900 mb. For most of the cloud layer, the updraft–downdraft model produces less drying through the moistening effect of enhanced detrainment. This indicates that the mass flux for low and middle clouds is enhanced. Figure 12 shows the time-averaged mass fluxes calculated with (Fig. 12a) the updraft-only model and (Fig. 12b) the updraft–downdraft model. Comparing the solid line appearing in the right half of Fig. 12a with the long-dashed line in Fig. 12b, we see that the updraft mass flux is considerably intensified at lower levels, indicating that relatively shallow clouds are enhanced.

The change of the spectral distribution of cumulus mass flux indicated above can be more directly seen in

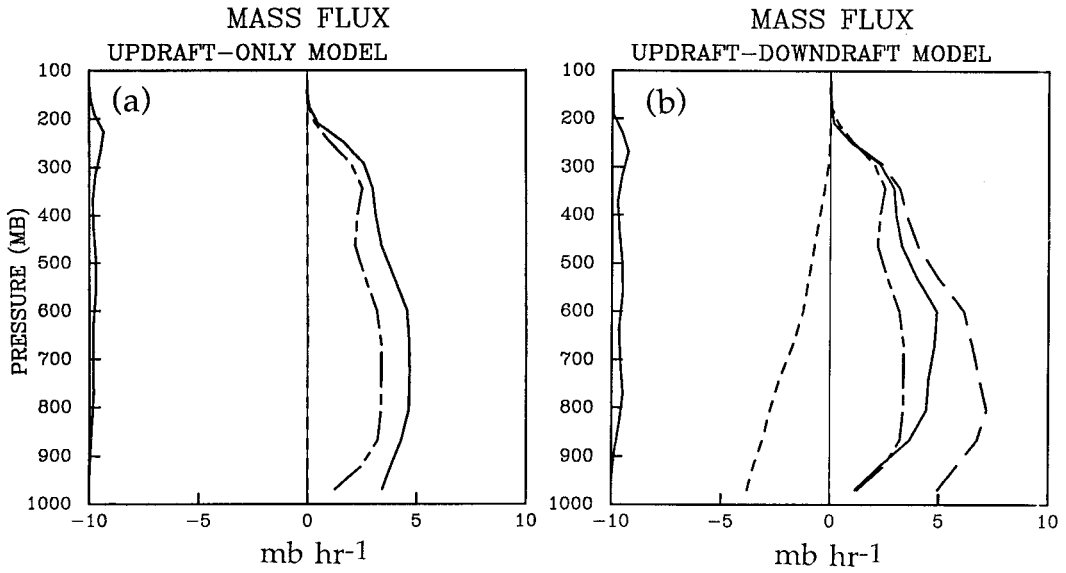

FIG. 12. Time-averaged mass fluxes calculated with (a) the updraft-only model and (b) the updraft–downdraft model. The identical chain lines in (a) and (b) show the observed large-scale upward mass flux. The solid line appearing in the right half of each panel shows the *net* upward cumulus mass flux, which is the updraft mass flux itself in (a) and the difference of the upward mass flux (long-dashed) and the downdraft mass flux (short-dashed) in (b). The solid line near the left edge of each panel shows the distribution of cloud base mass flux into different types of clouds as identified by cloud-top pressure shown by the ordinate.

TABLE 1. Normalized cloud work function A_N as a function of the pressure at cloud top based on the GATE phase II average (unit: J kg^{-1} mb^{-1}).

Cloud-top pressure	1	75	150	275	437.5	617.5	775	900	975
A_N	20	15	3.3898	1.128	0.507	0.150	0.084	0.072	0.066

Fig. 12. Comparing the solid line near the left edge of the panel between Figs. 11a and 11b, we see that middle and low clouds are, in fact, enhanced with the updraft–downdraft model. As pointed out near the beginning of this paper, downdrafts tend to decrease the cumulus drying above cloud base for a given updraft mass flux since the subsidence between clouds tends to be reduced. This decrease of cumulus drying, however, provides a more favorable environment for relatively shallow clouds and produces a feedback on the updraft mass flux through the enhancement of those clouds. The results shown above indicate that this feedback is primarily responsible for the difference of time-averaged cumulus drying effect.

7. Single-column prognostic tests

The semiprognostic test presented above directly examines the output of the cumulus parameterization Q_{1C} and Q_2 applied to each observation time. Since it does not integrate in time, there is no guarantee that the time-averaged tendencies are small so that the systematic error due to the parameterization can be seen in the time mean of the results in a way independent of any feedbacks. Moreover, as we did in section 6, it is rather straightforward to identify the contribution of each component in the parameterization to the total effect even when averaged in time. The semiprognostic test, however, does not tell how the errors of the prognostic variables evolve in time. This point is especially important in evaluating a cumulus parameterization since the net time change of those variables is usually a small difference of the cumulus and large-scale advection effects. Thus, as an intermediate approach between the semiprognostic and fully prognostic tests, the ''single-column prognostic test'' using a single-column model can be a useful approach of testing a cumulus parameterization (Emanuel et al. 1995).

To perform a single-column prognostic test of the revised A–S cumulus parameterization presented in this paper, we first calculate the time rate of advective changes of temperature and water vapor mixing ratio and radiative heating rates for the $1^\circ \times 1^\circ$ grid box at the center of the GATE network for every 3-h observation time. Using these prescribed advection and radiation effects linearly interpolated and the cumulus effects calculated from the cumulus parameterization, the thermodynamic and water-vapor budget equations are integrated in time. As in the semiprognostic tests, we assume that the lowest layer is the PBL and the level at the top of the layer is cloud base. Instead of using observed advective (and radiative) rates of change and a PBL parameterization, we mimic the entire PBL processes by predicting the temperature T and water-vapor mixing ratio q of the PBL adjusting toward observed values. For example, we predict q of the PBL through

$$q_B(n+1) - q_B(n) = -\alpha\Delta t[q_B(n) - q_B^*(n+1)], \quad (7.1)$$

where the subscript B denotes the PBL, q_B^* is the value of q_B interpolated from observation, α is the adjustment coefficient taken as 1 day^{-1}, n is the index for time level, and Δt is the time interval of the integration taken as 1 h.

Above the PBL, we first predict $\tilde{q}$, which is a temporary value of q without cumulus effects, through

$$\tilde{q}(n+1) = q(n) + \frac{\Delta t}{2}\left[\left(\frac{\partial q}{\partial t}\right)_{\text{adv}}^{n+1} + \left(\frac{\partial q}{\partial t}\right)_{\text{adv}}^{n}\right], \quad (7.2)$$

where $(\partial q/\partial t)_{\text{adv}}$ is the prescribed time rate of advective change of q. A similar procedure (except the prescribed radiative heating is included) is used to obtain $\tilde{T}$, which is the temporary value of T without cumulus effects. These values of $\tilde{q}$ and $\tilde{T}$ are used as inputs to the cumulus parameterization, which is identical to that we used for the semiprognostic tests described in section 6, except that the definition of the large-scale forcing is now through $F \equiv A - A_0$, where A is the cloud work function for the given profiles of q and T, and A_0 is the specified critical or equilibrium cloud work function. As in Lord et al. (1982), A_0 is given by

$$A_0 = A_N(p_B - p_T), \quad (7.3)$$

where p_B and p_T are pressures at cloud base and cloud top, respectively; A_N is the normalized critical cloud work function, which is a function of pressure at cloud top. For the tests described here, A_N for each cloud type is obtained through interpolation from the values given in Table 1, which is based on the average of the cloud work function calculated for individual soundings in the GATE Phase III dataset.

The A–S parameterization calculates $\Delta t(\partial T/\partial t)_{\text{cu}}$ and $\Delta t(\partial q/\partial t)_{\text{cu}}$, which are the required changes of T and q, respectively, for the adjustment of A to A_0 for all cloud types. Then, for example, q at time step $n+1$ after the adjustment, which is denoted by $\hat{q}$, is given by

$$\hat{q}(n+1) = \tilde{q}(n+1) + \beta\Delta t(\partial q/\partial t)_{\text{cu}}, \quad (7.4)$$

where β is a coefficient for relaxed adjustment, giving full adjustment at each time step when $\beta = 1$ and partial adjustment when $\beta < 1$. For the results shown below, we use $\beta = 1/3$, which corresponds to the adjustment time scale of 3 h. Finally, to control computational noise in the predicted vertical profiles, which is large when the vertical resolution is high, we effect smoothing

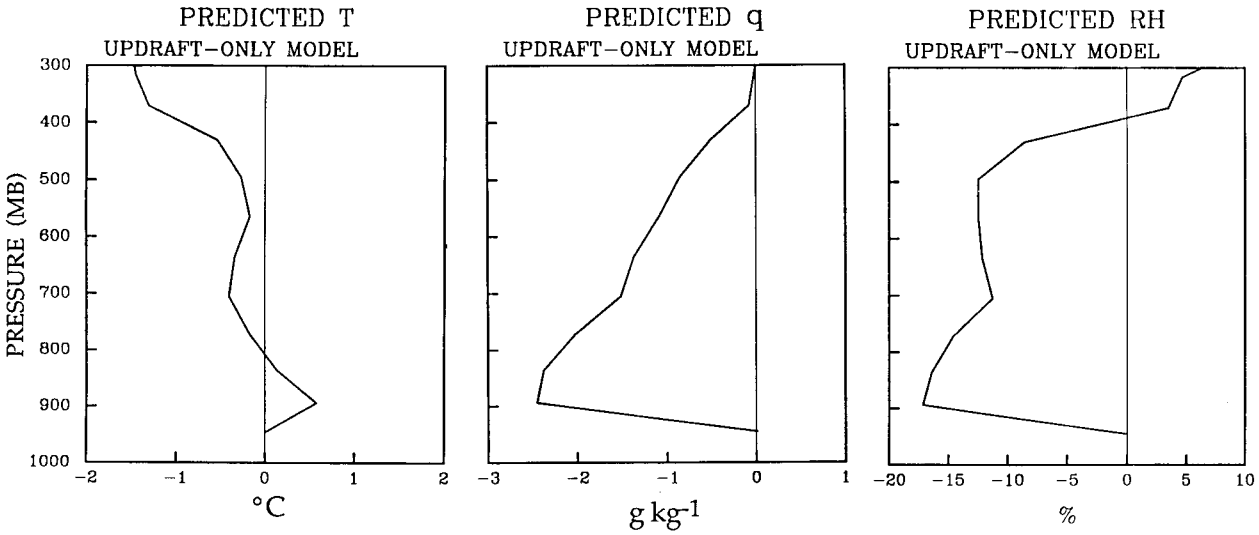

FIG. 13. Vertical profiles of the errors of T, q, and RH predicted with the updraft-only model averaged over the entire 18-day prediction period covering GATE Phase III.

through the vertical diffusion of q and T at each time step. For q, for example, the smoothing process is given by

$$q_k = \hat{q}_k + \frac{\kappa \Delta t}{(\rho \Delta z)_k}\left[\rho_{k-1/2}\frac{\hat{q}_{k-1} - \hat{q}_k}{(\Delta z)_{k-1/2}} - \rho_{k+1/2}\frac{\hat{q}_k - \hat{q}_{k+1}}{(\Delta z)_{k+1/2}}\right]. \tag{7.5}$$

We have used $\kappa = 2$ m^2 s^{-1} throughout the entire cloud layer.

Freezing processes within clouds are not explicitly included for both semiprognostic and single-column prognostic tests reported in this paper. In the single-column prognostic tests, however, the saturation water-vapor mixing ratio is calculated with respect to ice when the temperature is below 273 K. We further assume that, when the environmental relative humidity is higher than 90%, only a fraction of cloud water detrained from cloud top evaporates. Between 90% and 100% relative humidity, the fraction is assumed to linearly depend on the environmental relative humidity, with no evaporation when the environment is saturated. If supersaturation occurs, the excessive water vapor is assumed to condense and immediately fall to the ground.

Figure 13 shows the vertical profiles of the time-mean errors of T, q, and RH (relative humidity) predicted with the updraft-only model. The most serious mean errors appear in the q (and, correspondingly, RH) fields for the lower part of the column. This is consistent with the results of the semiprognostic test, which show that the updraft-only model tends to overestimate the cumulus drying effect at those levels (see Fig. 8a). Figure 14 shows the results from the updraft–downdraft model. Comparing this with Fig. 13, we see that the inclusion of downdraft effects drastically improves the results throughout the entire column, especially in its lower part.

Figure 15 shows the height–time sections of RH: Fig. 15a observed, Fig. 15b predicted with the updraft-only model, and Fig. 15c predicted with the updraft–downdraft model. In all of these panels, the observed time mean is subtracted. In Fig. 15b, we again see the trend for excessive drying with the updraft-only model. Figure 15c shows the results from the updraft–downdraft model. Large differences between Figs. 15c and 15a appear at upper levels, around 400 mb and above, where the predicted time changes are almost entirely due to the prescribed large-scale advection effects. This indicates that the source of errors is not in the parameterized cumulus effects. We also note that observed humidities are suspect at these levels. At middle and lower levels, on the other hand, fluctuations of RH are predicted reasonably well. There is, however, a tendency to overpredict the amplitude of the fluctuations.

The result of the ''relative-humidity test'' presented above is at least encouraging, although we find that it is rather sensitive to the choices of A_N and β. Currently we are studying the sensitivity in a systematic manner.

8. Updraft model with a simplified rainwater budget equation

The model described so far is extremely computer-time demanding, mainly because stationary solutions of the coupled rainwater and vertical momentum equations must be obtained by iteration for a range of the updraft tilting angle. Recently, we have developed a simplified, drastically more economical version of the model. The simplification is mainly through empirically specifying the vertical profile of the rainwater mixing ratio so that

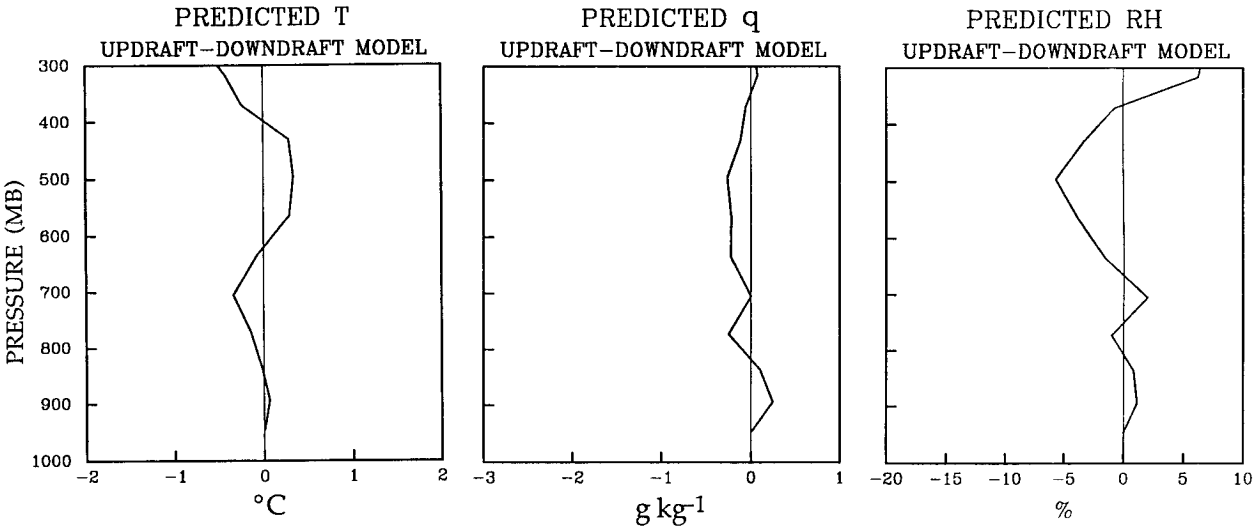

FIG. 14. As in Fig. 13 but predicted with the updraft–downdraft model.

we can only deal with the vertically integrated rainwater budget equation.

We express the rainwater mixing ratio as

$$q_r = \hat{q}_r N(z), \tag{8.1}$$

where $N(z)$ is an empirical function of height. Using (8.1) in (2.11), applied to cloud top denoted by subscript T, we may write

$$w_T = (a - b\hat{q}_r)^{1/2}, \tag{8.2}$$

where

$$a \equiv \frac{1}{\eta_T^2}\left[w_B^2 + \int_{z_B}^{z_T} 2\eta^2 \frac{B}{1+\gamma^*}\, dz\right],$$

$$b \equiv \frac{1}{\eta_T^2}\int_{z_B}^{z_T} 2\eta^2 \frac{gN}{1+\gamma^*}\, dz. \tag{8.3}$$

Integrating the rainwater budget equation (2.3) from cloud base to cloud top and using (8.1) and (8.2), we obtain

$$F \equiv \frac{\partial}{\partial t}\left(\int_{z_B}^{z_T} \frac{\eta}{w} q_r\, dz\right)$$

$$= \left[-c\sin\theta - d + \left(\frac{e}{(a - b\hat{q}_r)^{1/2}} - f\right)\cos^2\theta\right]\hat{q}_r + h. \tag{8.4}$$

Here $\rho\sigma/m_B = \eta/w$ has been used and

$$c \equiv \int_{z_B}^{z_T} \frac{2}{\lambda a}\frac{\eta}{w} N V_t\, dz,$$

$d \equiv \eta_T N(z_T) - \eta_B N(z_B)$, $e \equiv \eta_T N(z_T) V_t$, $f \equiv (\eta_B/w_B) \cdot N(z_B) V_t$, and $h \equiv 10\int_{z_B}^{z_T} \eta c_0 \ell\, dz$. We further simplify the problem by approximating w in c by w^*, where w^* is the updraft velocity calculated from (2.11) using $q_r = (\hat{q}_r)_0 N$, where $(\hat{q}_r)_0$ is an approximation to $\hat{q}_r$ given by

$$(\hat{q}_r)_0 = 0.75\frac{\displaystyle\int_{z_B}^{z_T} \eta B\, dz}{\displaystyle\int_{z_B}^{z_T} \eta g N\, dz}. \tag{8.5}$$

The numerator is the cloud work function (CWF) defined by A–S. The empirical factor 0.75 represents the amount of decrease of the CWF by the inclusion of rainwater drag. Then, once N is specified, the terms c, d, e, f, and g can be calculated without using the rainwater budget equation.

To specify $N(z)$, we assume that it is related to the local and upstream thermal buoyancy. At present we are using

$$N = \frac{1}{2}\left(\frac{B}{B_{\max}} + \frac{S}{S_{\max}}\right), \tag{8.6}$$

where $B_{\max}$ is the maximum value of the buoyancy,

$$S = \left[\frac{1}{\eta^2}\int_{z_B}^{z} \eta^2 B\, dz'\right]^{1/2} \tag{8.7}$$

represents the dependency of w to the upstream buoyancy, and $S_{\max}$ is the maximum value of S.

We require $q_r > 0$, $w_T \geq 0$, and that the rain flux at cloud top be nonnegative and that the rain flux at cloud base be nonpositive. We further require $\partial F/\partial\hat{q}_r \leq 0$ for stability. We are now interested in pairs of $\sin\theta$ and $\hat{q}_r$ that satisfy $F = 0$ and the conditions given above. We have found that generally there are two sets of solutions: one for $R_T > 0$ and the other for $R_T = 0$, where $R_T = q_r(w_T/\cos\theta - V_t\cos\theta)$ is the rain flux at cloud top. The set of solutions with $R_T > 0$ corresponds to the solutions for large tilting angles described in section 3, while

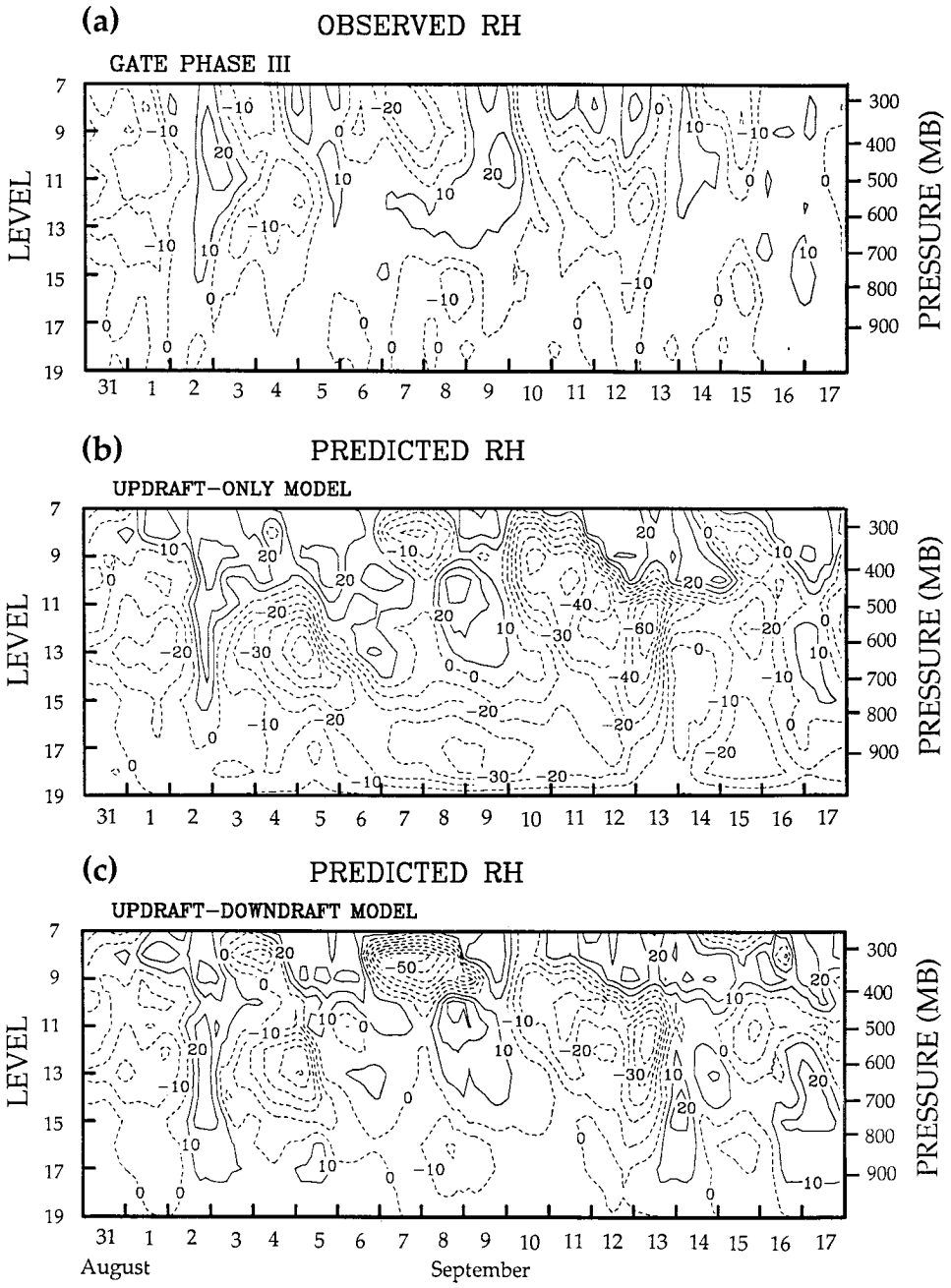

FIG. 15. Time–height sections of RH, (a) observed and predicted (b) with the updraft-only model and (c) with the updraft–downdraft model. The observed time mean is subtracted in all of the three panels. The vertical coordinate is shown using the integer index defined in section 3 with $N = 19$ (left) and pressure (right).

those with $R_T = 0$ corresponds to the solutions for small tilting angles. (In the present simplified system, however, the solutions for small tilting angles are not unstable because instability is associated with a highly localized perturbation of q_r, which is excluded by the specification of N.) Then, the solutions we are primarily interested in are those with $R_T > 0$ that satisfy $F = 0$ and $\partial F/\partial \hat{q}_r = 0$. (When solutions with $R_T > 0$ do not exist, the solution corresponding to the smallest $\hat{q}_r$ that satisfies $F = 0$ and $\partial F/\partial \hat{q}_r < 0$ is chosen.)

The results of the A–S cumulus parameterization scheme based on the simplified updraft–downdraft model have been compared with those from the original scheme semiprognostically, Figure 16 shows Phase III–averaged profiles of Q_{1C} and $-Q_2$ predicted with the simplified model. Comparing Fig. 16 to Fig. 8b, we see

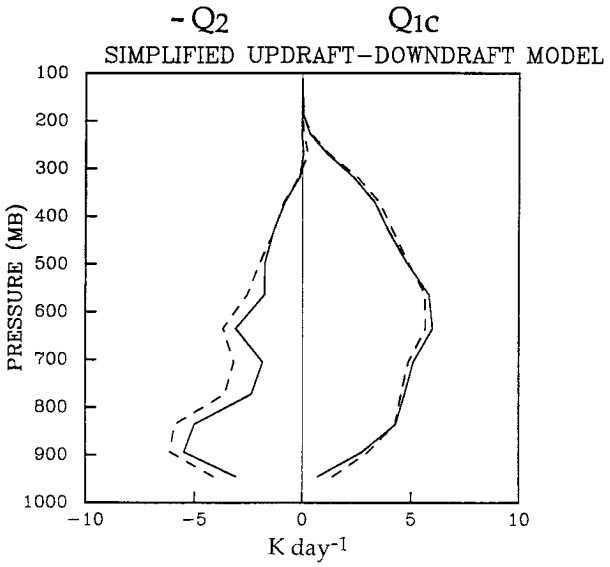

FIG. 16. As in Fig. 8b but predicted with the simplified model.

very little difference from the results with the original scheme in spite of about one order of magnitude reduction of computer time.

9. Summary and further comments

A combined updraft–downdraft model that includes the mass, rainwater, and vertical momentum budget equations for both updrafts and downdrafts is incorporated into the A–S cumulus parameterization. The rainwater budget equation in the model includes the loss of rainwater through the outgoing rain flux as well as the generation of rainwater and the in-cloud rain flux. This equation is coupled with the vertical momentum equation through the rain drag in the latter.

Stationary solutions of the coupled rainwater budget and vertical momentum equations are obtained numerically for a range of prescribed updraft tilting angle θ. Two types of stationary solutions are identified: *solutions for small tilting angles* and *solutions for large tilting angles.* These solutions represent different balances of the terms in the rainwater budget equation, and analysis of the stability with respect to a perturbation on the vertical distribution of rainwater shows that the solutions for small tilting angles are unstable, while the solutions for large tilting angles are stable. The instability of the solutions for small tilting angles is interpreted as a consequence of strong coupling of the rainwater budget and vertical momentum equations.

In practical applications of the combined updraft–downdraft model, we choose the smallest tilting angle in the stable range as an optimal value of θ. As far as θ is in that range, the precise choice of θ does not seem to be very important since the solutions for large tilting angles do not show much dependence on θ.

After we determine the updraft tilting angle for each subensemble identified by the vanishing buoyancy level, a downdraft model is used to find properties of the associated downdraft. In the model, downdrafts are assumed to be initiated and maintained by the loading and evaporation cooling of rainwater. With the known rain flux from updrafts, the mass, water vapor, moist static energy, total water, and vertical momentum of downdrafts are obtained for each subensemble by solving the corresponding budget equations. In formulating the vertical change of downdraft mass flux, we assume that the horizontal area covered by the downdraft is equal to the horizontal area covered by the rainfall outside the updraft. We consider three processes that can change this area with height: the increase of the area due to the tilt of the updraft, the decrease of the area due to the horizontal convergence of falling raindrops, and the decrease of the rain-covered area due to evaporation of raindrops along the edge of the downdraft. The entrainment and detrainment are then formulated through considering perturbation of cloud-scale horizontal velocity whose direction is randomly distributed. Admittedly, these formulations are crude and many of them are hypothetical. Yet the overall results for the downdrafts at lower levels seem to be quite reasonable (e.g., Fig. 13).

As in the original A–S parameterization, the cloud work function (CWF) quasi equilibrium is assumed for each subensemble. There is evidence that the CWF originally defined without rain-drag and downdraft effects can still be used in the revised parameterization.

The revised A–S parameterization is evaluated through semiprognostic and single-column prognostic tests using the GATE Phase III data. The updraft-only model predicts excessive cumulus drying in the lower part of cloud layer. This deficiency is almost completely eliminated by the inclusion of downdrafts by shifting a significant portion of cumulus drying downward from the cloud layer to the subcloud layer. It is interesting to see that the reduction of cumulus drying in the cloud layer is not simply through a reduction of cumulus subsidence. For most of the cloud layer, the updraft–downdraft model produces less drying due to the moisture detrainment from enhanced low and middle clouds. The result of ''relative humidity'' tests following the single-column prognostic approach is at least encouraging.

The model described in the main part of this paper is extremely computer-time demanding primarily because stationary solutions of the coupled rainwater and vertical momentum equations must be obtained by iteration for a range of the updraft tilting angle. A simplified and, therefore, drastically more economical version of the mode is also developed. The simplification is mainly through empirically specifying the vertical profile of the rainwater mixing ratio, so that we can only deal with the vertically integrated rainwater budget equation. The results of the A–S cumulus parameterization scheme based on the simplified updraft–downdraft model are very similar to those with the original

scheme in spite of about one order of magnitude reduction of computer time.

When we use the revised A–S parameterization described above in fully prognostic models such as GCMs, we need to introduce additional assumptions. Convective downdrafts may significantly modify the thermodynamical properties of the air in the PBL through the detrainment. This modification is usually drying (and cooling) of the PBL. In nature, however, these effects should be confined in relatively narrow regions near convective cells. Since the horizontal scale of this region is typically much smaller than the grid size of GCMs, and since the local heat and moisture fluxes at the surface should quickly respond to the modification of the PBL, the downdraft effects on the PBL should not be used to directly modify the values averaged over the entire grid box. At present, in our application of the model to the University of California, Los Angeles (UCLA) GCM, we assume that the downdraft effects on the PBL are locally compensated by enhanced latent (and sensible) heat fluxes from the underlying surface.

An example of the GCM results with an earlier version of the revised A–S cumulus parameterization is shown in Arakawa and Cheng (1993). In these results, the most visible improvement due to the inclusion of downdrafts appears over land, where the enhanced latent (and sensible) heat fluxes cool the ground temperature. Assessing the impact of this effect on overall simulations with the GCM, however, is complicated because the ground temperature also sensitively depends on the rest of the GCM, formulations of cloud–radiation interactions in particular.

Acknowledgments. The authors would like to thank Kerry Emanuel and two anonymous reviewers for their extensive reviews and numerous suggestions for improving the original manuscript. This research is supported by NSF Grant ATM-9224863, NASA Grant NAG5-2591, and NSC/ROC Grant 85-2111-M-052-001-AP4. All figures are prepared by Miss Yea-Ching Tung. Computations are performed at computer facilities at NCAR and UCLA Department of Atmospheric Sciences.

APPENDIX

Formulations of Entrainment and Detrainment for Downdraft

As in the text, let the inward components of the mean and perturbation cloud-scale velocities at the downdraft boundary be $\bar{u}$ and u' respectively. We assume $u' = U \sin\psi$, where $U(>0)$ and ψ are the magnitude and direction of the perturbation velocity, respectively. For $|\bar{u}| < U$, the sign of $\bar{u} + u'$ depends on ψ. It is clear that entrainment occurs when

$$-\sin^{-1}\left(\frac{\bar{u}}{U}\right) < \psi < \pi + \sin^{-1}\left(\frac{\bar{u}}{U}\right). \tag{A.1}$$

We assume that ψ is random with the probability function given by

$$\rho(\psi) = \frac{1}{2\pi}. \tag{A.2}$$

The expected rate of entrainment per unit height, ε, can be obtained by integrating the entraining mass weighted with its probability through the ranges of ψ given by (A.1). Thus we may write

$$\varepsilon = \int_{-\sin^{-1}(\bar{u}/U)}^{\pi+\sin^{-1}(\bar{u}/U)} \rho(\bar{u} + u')L_d\rho(\psi)\, d\psi. \tag{A.3}$$

Using $u' = U \sin\psi$ and (A.2), we can show that (A.3) gives

$$\varepsilon = \rho\bar{u}L_d\left[\frac{1}{2} + \frac{1}{\pi}\sin^{-1}\left(\frac{\bar{u}}{U}\right)\right] + \frac{\rho UL_d}{\pi}\left[\sin^{-1}\left(\frac{\bar{u}}{U}\right)\right]. \tag{A.4}$$

For convenience, we further rewrite (A.4) as

$$\varepsilon = \left\{\frac{1}{2} + \frac{1}{\pi}\sin^{-1}\left[\frac{\partial m/\partial z}{(\partial m/\partial z)_0}\right]\right\}\frac{\partial m}{\partial z} + \frac{1}{\pi}\left\{\left(\frac{\partial m}{\partial z}\right)_0^2 - \left(\frac{\partial m}{\partial z}\right)^2\right\}^{1/2}, \tag{A.5}$$

where $\partial m/\partial z = \rho\bar{u}L_d$ [see (4.18)] is the rate of net entrainment and $(\partial m/\partial z)_0 \equiv \rho UL_d$ is used as a reference rate of net entrainment. Here, for simplicity, we ignored the difference between $\partial m/\partial z$ and $(\partial m/\partial z)_{\text{conv}}$. The relation $\cos[\sin^{-1}(\bar{u}/U)] = (U^2 - \bar{u}^2)^2/U$ has also been used in deriving (A.5).

For $|\bar{u}| < U$, detrainment from the downdraft occurs when

$$\pi + \sin^{-1}\left(\frac{\bar{u}}{U}\right) < \psi < 2\pi - \sin^{-1}\left(\frac{\bar{u}}{U}\right). \tag{A.6}$$

Then, the expected rate of detrainment per unit height, δ, can be obtained following a procedure similar to that for (A.5). The result is

$$\delta = \left\{-\frac{1}{2} + \frac{1}{\pi}\sin^{-1}\left[\frac{\partial m/\partial z}{(\partial m/\partial z)_0}\right]\right\}\frac{\partial m}{\partial z} + \frac{1}{\pi}\left\{\left(\frac{\partial m}{\partial z}\right)_0^2 - \left(\frac{\partial m}{\partial z}\right)^2\right\}^{1/2}. \tag{A.7}$$

We currently relate $(\partial m/\partial z)_0$ to the rate of mass entrainment of the associated updraft, λ, by $(\partial m/\partial z)_0 = \pi\lambda/2$. This ad hoc relation roughly corresponds to the assumption that the downdraft and associated updraft share the same value of U and have approximately equal horizontal length of the interface with the cloud environment.

REFERENCES

Arakawa, A., and W. H. Schubert, 1974: Interaction of a cumulus cloud ensemble with the large-scale environment. Part I. *J. Atmos. Sci.*, **31,** 674–701.

——, and M.-D. Cheng, 1993: The Arakawa–Schubert cumulus parameterization. *The Representation of Cumulus Convection in Numerical Models of the Atmosphere, Meteor. Monogr.*, No. 46, Amer. Meteor. Soc., 123–136.

Cheng, M.-D., 1989a: Effects of downdrafts and mesoscale convective organization on the heat and moisture budgets of tropical cloud clusters. Part I: A diagnostic cumulus ensemble model. *J. Atmos. Sci.,* **46,** 1517–1538.

——, 1989b: Effects of downdrafts and mesoscale convective organization on the heat and moisture budgets of tropical cloud clusters. Part II: Effects of convective downdrafts. *J. Atmos. Sci.,* **46,** 1540–1564.

——, and M. Yanai, 1989: Effects of downdrafts and mesoscale convective organization on the heat and moisture budgets of tropical cloud clusters. Part III: Effects of mesoscale convective organization. *J. Atmos. Sci.,* **46,** 1566–1588.

——, and A. Arakawa, 1990: Inclusion of convective downdrafts in the Arakawa–Schubert cumulus parameterization. Tech. Rep., 69 pp. [Available from Department of Atmospheric Sciences, 405 Hilgard Avenue, University of California, Los Angeles, CA 90095.]

——, and ——, 1991a: Inclusion of convective downdrafts in the Arakawa–Schubert cumulus parameterization. *Extended Abstracts, 19th Conf. on Hurricanes and Tropical Meteorology,* Miami, FL, Amer. Meteor. Soc., 295–300.

——, and ——, 1991b: Inclusion of rainwater budgets and convective downdrafts in a cumulus parameterization. Preprints, *Ninth Conf. on Numerical Weather Prediction,* Denver, CO, Amer. Meteor. Soc., 99–102.

——, and ——, 1993: A cumulus parameterization with rainwater budget and convective downdrafts. *Extended Abstracts, 20th Conf. on Hurricanes and Tropical Meteorology,* San Antonio, TX, Amer. Meteor. Soc., 83–90.

——, and ——, 1994: Effects of including convective downdrafts and a finite cumulus adjustment time in a cumulus parameterization. Preprints, *10th Conf. on Numerical Weather Prediction,* Portland, OR, Amer. Meteor. Soc., 102–104.

——, and ——, 1997: Computational procedure for the Arakawa–Schubert cumulus parameterization. Tech. Rep., 70 pp. [Available from Department of Atmospheric Sciences, 405 Hilgard Avenue, University of California, Los Angeles, CA 90095.]

Cox, S. K., and K. T. Griffith, 1978: Tropospheric radiative divergence during Phase III of the GARP Atlantic Tropical Experiment (GATE). Atmospheric Science Paper No. 291, 166 pp. [Available from Department of Atmospheric Science, Colorado State University, Fort Collins, CO 80523.]

——, and ——, 1979: Estimates of radiative divergence during Phase III of the GARP Atlantic Tropical Experiment. Part I: Methodology. *J. Atmos. Sci.,* **36,** 576–585.

Emanuel, K. A., 1986: Some dynamical aspects of precipitating convection. *J. Atmos. Sci.,* **43,** 2183–2198.

——, 1991: A scheme for representing cumulus convection in large-scale models. *J. Atmos. Sci.,* **48,** 2313–2335.

——, P. C. Joss, and M. Zivkovic, 1995: Optimization and validation of convective representations. *Extended Abstracts, 21st Conf. on Hurricanes and Tropical Meteorology,* Miami, FL, Amer. Meteor. Soc., 184–185.

Ferrier, B. S., and R. A. Houze, 1989: One-dimensional time-dependent modeling of GATE cumulonimbus convection. *J. Atmos. Sci.,* **46,** 330–352.

Frank, W. M., and C. Cohen, 1987: Simulation of tropical convective systems. Part I: A cumulus parameterization. *J. Atmos. Sci.,* **44,** 3787–3799.

Fritsch, J. M., and C. F. Chappell, 1980: Numerical prediction of convectively driven mesoscale pressure systems. Part I: Convective parameterization. *J. Atmos. Sci.,* **37,** 1722–1733.

Grell, G., 1993: Prognostic evaluation of assumptions used by cumulus parameterization. *Mon. Wea. Rev.,* **121,** 764–787.

——, Y.-H. Kuo, and R. J. Pasch, 1991: Semiprognostic tests of three cumulus parameterization schemes in middle latitudes. *Mon. Wea. Rev.,* **119,** 5–31.

Haman, K. E., and M. Niewiadomski, 1980: Cold downdrafts in cumulonimbus clouds. *Tellus,* **32,** 525–536.

Houze, R. A., Jr., 1989: Observed structure of mesoscale convective systems and implications for large-scale heating. *Quart. J. Roy. Meteor. Soc.,* **115,** 425–462.

Johnson, R. H., 1976: The role of convective-scale precipitation downdrafts in cumulus and synoptic-scale interactions. *J. Atmos. Sci.,* **33,** 1890–1910.

——, 1980: Diagnosis of convective and mesoscale motions during Phase III of GATE. *J. Atmos. Sci.,* **37,** 733–753.

Kao, C.-Y., and Y. Ogura, 1987: Response of cumulus clouds to large-scale forcing using the Arakawa–Schubert cumulus parameterization. *J. Atmos. Sci.,* **44,** 2437–2458.

Knupp, K. R., and W. R. Cotton, 1985: Convective cloud downdraft structure: An interpretive survey. *Rev. Geophys.,* **23,** 183–215.

Lord, S. J., 1982: Interaction of a cumulus cloud ensemble with the large-scale environment. Part III: Semiprognostic test of the Arakawa–Schubert cumulus parameterization. *J. Atmos. Sci.,* **39,** 88–103.

——, and A. Arakawa, 1980: Interaction of a cumulus cloud ensemble with the large-scale environment. Part II. *J. Atmos. Sci.,* **37,** 2677–2692.

——, W. C. Chao, and A. Arakawa, 1982: Interaction of a cumulus cloud ensemble with the large-scale environment. Part IV: The discrete model. *J. Atmos. Sci.,* **39,** 104–113.

Molinari, J., and T. Corsetti, 1985: Incorporation of cloud-scale and mesoscale downdrafts into cumulus parameterization: Results of one- and three-dimensional integrations. *Mon. Wea. Rev.,* **113,** 485–501.

Moorthi, S., and M. J. Suarez, 1992: Relaxed Arakawa–Schubert: A parameterization of moist convection for general circulation models. *Mon. Wea. Rev.,* **120,** 978–1002.

Ogura, Y., and T. Takahashi, 1971: Numerical simulation of the life cycle of a thunderstorm cell. *Mon. Wea. Rev.,* **99,** 895–911.

Pan, H.-L., and W.-S. Wu, 1994: Implementing a mass flux convective parameterization package for the NMC medium-range forecast model. Preprints, *10th Conf. on Numerical Weather Prediction,* Portland, OR, Amer. Meteor. Soc., 96–98.

Payne, S. W., 1981: The inclusion of moist downdraft effects in the Arakawa–Schubert cumulus parameterization. Preprints, *Fifth Conf. on Numerical Weather Prediction,* Monterey, CA, Amer. Meteor. Soc., 277–284.

Seitter, K. L., and H.-L. Kuo, 1983: The dynamical structure of squall-line thunderstorms. *J. Atmos. Sci.,* **40,** 2831–2854.

Simpson, J., and V. Wiggert, 1969: Models of precipitating cumulus towers. *Mon. Wea. Rev.,* **97,** 471–489.

Soong, S.-T., and Y. Ogura, 1973: A comparison between axisymmetric and slabsymmetric cumulus cloud model. *J. Atmos. Sci.,* **30,** 879–893.

Srivastava, R. C., 1985: A simple model of evaporatively driven downdraft: Application in microburst downdraft. *J. Atmos. Sci.,* **42,** 1004–1023.

——, 1987: A model of intense downdrafts driven by the melting and evaporation of precipitation. *J. Atmos. Sci.,* **44,** 1752–1773.

Sud, Y. C., and G. K. Walker, 1993: A rain evaporation and downdraft parameterization to complement a cumulus updraft scheme and its evaluation using GATE data. *Mon. Wea. Rev.,* **121,** 3019–3039.

Sui, C.-H., M.-D. Cheng, X. Wu, and M. Yanai, 1989: Cumulus ensemble effects on the large-scale vorticity and momentum fields of GATE. Part II: Parameterization. *J. Atmos. Sci.,* **46,** 1609–1629.

Yanai, M., S. Esbensen, and J.-H. Chu, 1973: Determination of bulk properties of tropical cloud clusters. *J. Atmos. Sci.,* **30,** 611–627.